Identification of Slow Dynamic Processes in Poly(*n*-hexyl Methacrylate) by Solid-State 1D-MAS Exchange NMR

Ovidiu Pascui, Mario Beiner, and Detlef Reichert*

Martin-Luther-University Halle-Wittenberg, Department of Physics, Friedemann-Bach Platz 6, 06108 Halle/Saale, Germany

Received August 2, 2002

ABSTRACT: The molecular dynamics of the different molecular subunits in the amorphous polymer poly(*n*-hexyl methacrylate), PnHMA, was investigated by recently developed solid-state 1D-MAS exchange NMR methods at temperatures close to the glass transition temperature. The molecular mobility of main-chain, side-chain, and carboxyl carbons could be assigned to different relaxation processes as identified by dielectric and mechanical relaxation spectroscopy as well as caloric methods. Information about both the time constants as well as the geometry of the processes could be obtained. It was found that the side chain contributes in the dynamic window of NMR exchange experiments ($\tau_c \approx 1$ ms to 0.1 s) mainly to the β process while the main chain and carboxyl group are found to contribute to both the β and α processes. The data suggest that the contributions of side and main chain to the β process are qualitatively different. All dynamic processes exhibit a wide distribution of correlation times. The proper separation of spin-exchange processes from the molecular dynamics is demonstrated.

Introduction

Molecular dynamic processes in solid organic matter are commonly characterized in terms of their time scale as well as their geometry. The former is parametrized as jump rate k or correlation time, τ_c while the latter—when obtained from NMR experiments—is either quantified in terms of order parameters in cases where the actual topology could not be specified or as Euler angles relating the different sites that a probe molecule can occupy in the course of the dynamic process. In amorphous material where the local structure is disordered, the accurate characterization of the topology is difficult and often left to terms like "large-angle jump", "small-angle librations", or "rotational diffusion". The molecular dynamic processes in organic solids cover a dynamic range of many orders of magnitude which can experimentally be accessed by the well-know relaxation methods like dielectric and mechanical relaxation spectroscopy. Although the latter became almost routine methods, they have two crucial drawbacks. First, they are often not able to provide the dynamic information with molecular resolution; i.e., they cannot assign the detected dynamic processes to different parts of the molecular structure. Dielectric relaxation might serve as an example: here, the probe is the dipole moment that is attached to polar groups. Nonpolar groups like aliphatic chains are hardly detectable. Thus, the obtained dynamic information cannot strictly be assigned to the dynamics of the entire molecule but only to those part of the molecule to which the dipole moment is attached. NMR, however, can provide molecular-level resolution since its probes are the nuclear spins attached to single nuclei. Second, the relaxation methods do not provide accurate information about the geometry of the dynamic process, i.e., about jump angles or number of sites that can be occupied by the process. Although this is in general of minor interest only, it provides another valuable piece of information to characterize the dynamic process and is thus desirable to obtain.

Dynamic processes in polymers that occur in the "slow-motion regime", i.e., with correlation times on the order of milliseconds or longer, are of particular interest, since they determine the properties of the materials. Examples are transport properties in nanoporous materials[1,2] or organic conductors,[3] the mechanical properties of functional polymers (see for example ref 4), and the biologic activities of biopolymers.[5,6] Molecular motions that fall in this time scale are conveniently detectable by solid-state exchange NMR techniques which are sensitive to dynamic processes that occur with τ_c slower than the spin−spin relaxation time T_2 (typically on the order of milliseconds) but faster than the spin−lattice relaxation time T_1 (typically seconds). These exchange experiments are basically two-dimensional experiments (2D) where the intensity of the signals off the diagonal of the 2D spectrum is proportional to the share of nuclei that occupies different sites before and after an adjustable mixing periods t_m ($T_2 < t_m < T_1$). The experiment has to be repeated for a number of mixing periods, resulting in a number of 2D spectra with a growth of the off-diagonal signal with increasing length of t_m. The dependence of off-diagonal intensity vs t_m has to be fitted to a suitable analytical[7] or numerical[8] function in order to extract dynamic parameters. Since the introduction of this method,[9] there have been numerous applications for solids, too, in particular for organic crystals and polymers (for a review, see ref 10). Here, orientation-dependent NMR interaction like the chemical-shift anisotropy (CSA) or the quadrupolar interaction allows the observation of reorientations of the sample nucleus. This experiment provides accurate information about the geometry of the process that can be obtained from the 2D pattern of the exchange signals while information about the time scale is much harder to obtain, due to the sometimes weak exchange signals. The experiment might also suffer from the overlap of different NMR resonance lines or powder

* Corresponding author. E-mail: reichert@physik.uni-halle.de.

10.1021/ma0212442 CCC: $25.00
Published on Web 04/15/2003

patterns that make a detailed interpretation of the data impossible. Thus, it became customary to use selectively deuterated substances to avoid this spectral overlap. Although the deuteron is particularly useful for this kind of experiments,[11,12] it requires the demanding chemical synthesis of labeled compounds which restricts the applicability of the method. The ^{13}C nucleus is another promising candidate for these experiments since most of the synthetic polymers consist of hydrocarbon chains. To avoid the overlap of signals belonging to different carbon nuclei, one conveniently uses the magic-angle spinning technique (MAS) and can conduct 2D-MAS exchange experiments.[13−15] In these experiments, the broad resonances are condensed into few narrow spinning-sidebands (ssb) of which the central one (of order $N = 0$) appears at the position of the isotropic chemical shift. The ssb are separated from each other by the MAS spinning rate and cover a frequency range that is approximately equal to the range of the anisotropic chemical shift. The MAS method provides both increased spectral resolution and a much improved signal-to-noise ratio, which in turn enables a more accurate determination of the time scale of the process. Although the geometric information does not show up as clear as in the static experiments, it is still contained in the 2D spectra and cases were reported where this information was extracted.[16,17] The power of this experiment is certainly its ability to display the exchange pathway in cases when the molecular process involves alterations of the chemical identity of the nuclei.[18,19] The determination of exchange rates was also reported.[16,20] However, although the signal-to-noise of 2D-MAS experiments is superior to those of static 2D-exchange experiments, the quality of the signal does not permit an unambiguous investigation of more complex processes as they occur in polymers. For that, a more time saving NMR exchange method must be found that permits a better signal-to-noise ratio per machine time.

A promising way to do so is to reduce the dimensionality of the experiment, i.e., to reduce the 2D to a 1D experiment. While the indirect dimension has to be sampled in a time-consuming fashion in the 2D-exchange experiment, the idea of 1D-exchange experiments is to create a nonequilibrium state in the spin system that is sensitive to the mutual orientations of the nuclei. Any dynamic process that changes this orientation, i.e., a molecular reorientation, will disturb this state and should be detectable in the NMR signal. Such an experiment was introduced first in 1985.[21] It utilizes a TOSS (total suppression of spinning-side bands) sequence[22,23] to create a spin state that produces a MAS spectrum in which all ssb but that of order $N = 0$ have vanished. A molecular reorientation shows up in a reintroduction of the $N \neq 0$ ssb and their gradual growth with increasing length of t_m. However, the TOSS sequence is rather sensitive to experimental artifacts and leads typically to a loss of signal intensity. This is likely the reason why this clever method has found only few applications.[24,25] Some time has passed until a more promising method, baptized ODESSA (one- dimensional exchange spectroscopy by side band alternation),[26] was introduced. It does not utilize a complicated and sensitive building block but creates the necessary spin state by just a delay during which the magnetization evolves such that all odd-numbered ssb are inverted. Any reorientation of the probe nucleus alters the line intensities. While the ODESSA method works for samples with a single resonance only and is thus not applicable to polymers, its further development, time-reverse ODESSA (trODESSA),[27] works fine even for an arbitrary number of resolved resonances. Recently, another technique called CODEX (center-band only detection of exchange)[28,29] was introduced. It is similar to trODESSA but utilizes additional π-pulses to recouple the CSA which on one hand provide clearer and even additional information but reduce the signal intensity on the other hand (see below). For a summary and comparison of the different MAS exchange techniques, the interested reader is referred to ref 7.

In this paper, we will present 1D-MAS exchange experiments that utilize both the trODESSA and CODEX methods for the investigation of the molecular dynamics in the amorphous polymer poly(*n*-hexyl methacrylate). This sample was chosen since it belongs to the same interesting class of polymethacrylates like poly(methyl methacrylate) (PMMA) and poly(ethyl methacrylate) (PEMA), on which extensive NMR experiments were performed.[30−33] The molecular dynamics of these polymers depends on the length of the alkyl side chain. The interesting crossover region, where the relaxation times of the α and β relaxation approaches each other, occurs for PHMA[34,55] in a frequency range that is particularly suitable for MAS exchange NMR experiments. A summary of relaxation experiments in the crossover region of several poly(alkyl methacrylates) is given in ref 34. In this paper, we are interested in the molecular origin of the different molecular processes that were detected by conventional relaxation methods. Thus, we focus our attention in particular on the determination of the time constants for the different molecular dynamic processes of the main and side chain as well as on the carboxyl group that interconnects them. These data will be discussed in comparison to data obtained from dielectric, dynamic mechanical, and heat capacity spectroscopy. Some results aimed to determine the geometry of the observed processes will be discussed.

Experimental Section

PHMA was obtained from Dr. G. Meier (MPI Mainz/FZ Jülich) and used without further treatment. The glass-transition temperature was determined by DSC to be −19 °C. Additional information about the sample are given elsewhere.[34]

The NMR data were acquired on a Varian INOVA 400 spectrometer, equipped with a standard 7 mm Varian VT-CPMAS probe, as well as on a Varian UNITY 200, equipped with a 7 mm DOTY Super-Sonic VTMAS probe. Typical pulse length for both ^1H and ^{13}C were about 3.7 and 4.3 μs, respectively. We applied constant-amplitude CP and CW ^1H decoupling of about 34 kHz (200 MHz) and 75 kHz (400 MHz), respectively, during the evolution and acquisition periods. The actual sample temperature was carefully calibrated for each spin rate by a standard procedure.[35] ^{13}C-T_1 values were determined using the method described in ref 36. As 1D-MAS NMR exchange methods, we used both trODESSA as well as CODEX. Both methods have in common that they utilize magic-angle spinning (MAS) to facilitate spectral resolution and to retrieve dynamic information by comparing the orientation of the probe nucleus before and after an adjustable mixing period, t_m. This orientation is encoded in the NMR resonance frequency that is determined by the CSA of the probe nucleus and which evolves during the $T_R/2$ periods before and after t_m in the case of trODESSA. For CODEX, this dephasing of the magnetization is enhanced by applying trains of rotor-synchronized π-pulses during the evolution periods.[29] If no dynamic process happens, the orientation of the probe nucleus before and after t_m is the same and a NMR signal with full

intensity is acquired. If, however, the anisotropic frequencies of the probe nucleus changed due to a molecular reorientation during t_m, only part of the magnetization is refocused and thus, a decay in the signal intensity of the resonance line belonging to the reorienting nucleus is observed. The experiment is conducted for a number of logarithmically spaced mixing periods, starting from the minimum value of one T_R (typically hundreds of microseconds) and running up to typically some hundreds of milliseconds or a few seconds. The plot of the line intensities of the different resonances vs t_m (which we called from now on "the exchange decay") is analyzed in terms of decaying exponential (or other appropriate) functions to extract dynamic information; see below.

For the theory and experimental details, we refer to the original papers[27−29] describing the methods. However, some comments on experimental details are in order.

•The trODESSA experiment is the most economic experiment in terms of signal intensity since it requires, as compared to a simple CPMAS experiment, only two additional $\pi/2$ pulses, an additional T_2-active delay of length one T_R and the combination of two separate experiments to acquire the full complex signal information from the first evolution delay. However, it works well only if the dephasing of the anisotropic chemical shift during the evolution periods is sufficiently strong, i.e., if the ratio of the value of the CSA (in frequency units), $\Delta\sigma$, to the MAS spin rate, ν_R, is not smaller than approximately 2 (i.e., in the case of slow MAS) and if the dynamic process leads to a sufficiently large change of the CSA- tensor orientation, i.e., if the reorientation angles are sufficiently large. In contrast, CODEX can compensate for a sometimes unavoidable large ν_R and/or dynamic processes involving small angular changes by applying a larger number of π-pulses during the evolution periods. However, the latter is on the expense of signal intensity that in most practical cases deteriorates quickly if more than few π-pulse cycles are applied. The situation is even worse in cases of polymeric systems where relatively broad lines are found that decay quickly by T_2 relaxation, see below. This means that the investigator is prompted to choose the right experiment for the actual case: trODESSA for spectrally isolated lines with large CSA and/or a sufficiently large reorientation angle and CODEX for nuclei for which the resonance lines appear in crowded spectral ranges, having small CSA and/or small reorientation angles. Examples for the former are the carboxyl carbons in the samples under investigations while the latter case is typical for the aliphatic carbons.

• During t_m, the magnetization of the probe nucleus is subjected to exchange processes and decays to zero due to T_1 relaxation. In the original papers,[28,29] the CODEX sequence is augmented by a second mixing period, t_z, which is kept as short as possible (typically one T_R) while the first one, t_m, is arrayed as described above. The same approach can be applied to trODESSA experiments. Since there is no extra evolution of the magnetization before the second mixing period, t_z is not sensitive to exchange but to T_1 relaxation only. The experiment is now performed such that for each value of t_m, two separate sets of experiments are performed: the so-called exchange experiment with t_m first and t_z second and a reference experiment where the length of the first mixing period is set to t_z and those of the second to t_m. The purpose is that the reference experiment utilizes exactly the same delays and number of pulses as the exchange experiment but is sensitive to T_1 only and not to exchange. Dividing the line intensities of the two experiments eliminates the T_1 from the exchange decay and provides a normalized exchange decay; see Figure 1. In other words, the data obtained by this approach are "internally normalized". However, the effect of T_1 can also easily be eliminated by performing a separate T_1 experiment and multiplying the exchange decay by e^{t_m/T_1}. The latter approach saves machine time since (i) the extra T_1 experiment can typically be performed in about 10% of the time that is required for a separate reference experiment and (ii) the pulse sequences equipped with a second mixing time (like Figure 2b) do not provide the same signal intensity as the sequence without (like Figure 2a) since they require a larger number of pulses. It might also be of advantage to know the T_1 value in advance, for example to decide on the range of mixing times at which it is feasible to run the exchange experiment (there is not much meaning to run exchange experiments at values of t_m that exceed T_1). The investigator is prompted again to evaluate the pros and cons of the both approaches and to decide if the "internally normalized" or the nonnormalized types of experiments serve the purpose better for the actual case.

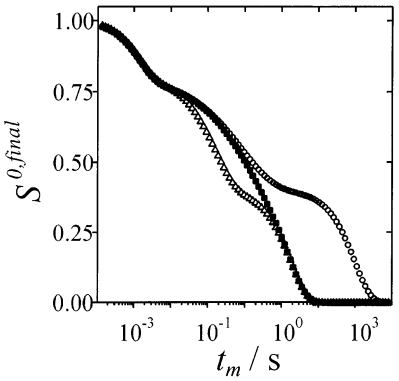

Figure 1. Schematic exchange decay. Full symbols: exchange decay typical for organic solids in natural ^{13}C abundance. Dispersions are due to a molecular process with $\tau_c \approx 1$ ms, spin diffusion with $\tau_{SD} \approx 1$ s and spin−lattice relaxation with $T_1 \approx 10$ s. Open triangles: schematic decay for ^{13}C-enriched solids where the spin-diffusion time constant has shortened by a ratio of about five. Open circles: schematic exchange decay for a natural abundance solid with an extreme T_1 of about 1000 s.

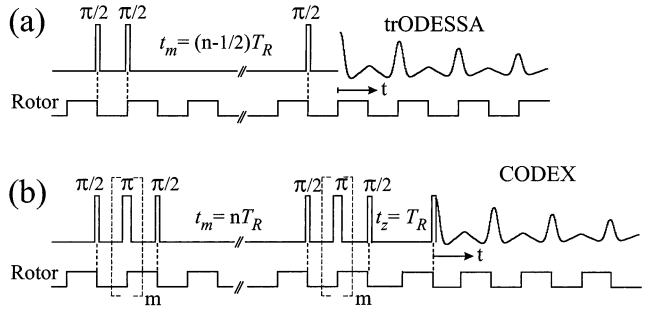

Figure 2. NMR-pulse sequences: trODESSA (a) and CODEX (b). The square wave below is the signal from the spinning MAS rotor. Note that for both experiments the length of the mixing periods t_m and the π-pulse cycles for CODEX has to be synchronized with the MAS rotation. The number of π-pulses, m, relates to the number of evolution cycles, N, as $N = (m + 1)/2$ ($m > 0$). The CODEX experiment is shown in a version with a second mixing period t_z that permits the acquisition of normalized exchange decays and compensates for T_1 relaxation (for details see text).

• While for a fixed MAS-spin rate, a trODESSA data set depends on one parameter only (t_m), the CODEX depends on the number of π-pulses in the evolution periods before and after t_m, too. In addition to the enhancement of the dephasing of the signal, such NT_R dependencies (acquired at a fixed, sufficiently large value of t_m) provide the additional opportunity to extract information about the topology of the monitored process.[28,29,37] However, a quantitative evaluation depends crucially on the knowledge of the relation between the CSA tensor and the molecule, which is not exactly known in most cases. Thus, we will focus on the determination of time constants, rather than geometric parameters but will make use of NT_R-dependencies to qualitatively characterize the dynamic process.

Interpretation of NMR parameters

The normalized exchange decay has the same time dependence as the correlation function of motion. This

can easily be explained by the fact that the exchange decay of a resonance line (ssb order N) can be written as[7]

$$s^N(t_m) = \sum_{i,j=1}^{n} I_{ij}^N P_{ij}(t_m) P_j(0) e^{-(t_m/T_1{}^j)} \quad (1)$$

where $I_{ij}{}^N$ are the NMR subspectra of the nuclei which have been at site j before and at site i after t_m, $P_{ij}(t_m)P_j(0)$ are the fractional populations of these species, and n is the number of distinguishable sites that can be occupied by the probe nucleus. The $I_{ij}{}^N$ can be calculated if knowledge about the mutual orientations of the CSA tensors at the different sites is available (which is often not the case for amorphous materials like polymers). On the other hand, the well-known correlation function of motion for a stochastic dynamic process is defined as

$$s(\tau) = \langle \theta(t')\theta(t'+\tau) \rangle_{t'} \quad (2)$$

with $\langle ... \rangle_{t'}$ being the time average. For a random symmetric two-site jump process involving sites at which the dynamic variable θ acquires values $\pm\theta_0$, eq 2 acquires the form

$$s(\tau) = {\theta_0}^2 \sum_{i,j=1}^{2} (-1)^{i-j} P_{ij}(\tau) P_j(0) \quad (3)$$

From a comparison of eqs 1 and 3, it is immediately clear that data obtained from NMR exchange experiments, corrected for the effect of T_1 relaxation, has the same time dependence as the correlation function of motion. Thus, NMR exchange experiments deliver directly a result that is proportional to the correlation function and do not require any model assumptions and recalculation as—for example—NMR-relaxation experiments do.

$P_{ij}(t_m)$ in eq 1 can be calculated from the knowledge of the exchange matrix. For a dynamic process in which the probe nucleus jumps with a rate k between n equally populated sites, the solution of eq 1 yields

$$s^N(t_m) = (b^N + c^N e^{-(t_m/\tau_c)}) e^{-(t_m/T_1)} \quad (4)$$

with[38]

$$\tau_c = \frac{1}{nk}$$

In amorphous systems, however, the correlation function often cannot be described as a single-exponential decay. In such cases, it is customary to replace the exponential function in eq 4 by a Kohlrausch–Williams–Watts (KWW) or stretched-exponential function.[39,40] Omitting the contribution from T_1 relaxation and normalizing the data yields

$$\frac{S}{S_0}(t_m) = \frac{s^N(t_m)}{{s_0}^N(t_m)} = (1 - a^N + a^N e^{-(t_m/\tau_c)^\beta}) \quad (5)$$

where ${s_0}^N(t_m)$ is the line intensity in the reference experiment as described above. From now on, we will call the parameter a^N the "exchange intensity". In all cases presented here, we will plot the intensity of the central ssb ($N = 0$). We will thus drop the index N in this section. The parameter β ($0 < \beta \leq 1$) is a measure for the widths of the distribution: $\beta = 1$ means the process can be described by a single correlation time τ_c while a smaller value of β means there is a distribution of τ_c.

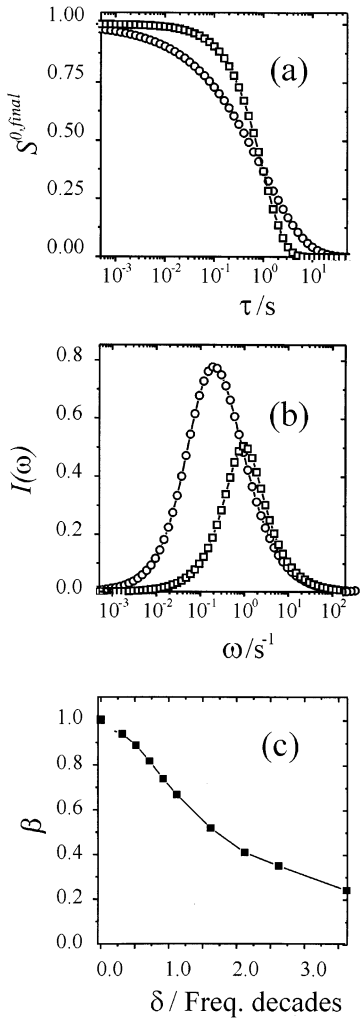

Figure 3. Schematic correlation function (a) and spectral density (b). Open squares: the correlation function is an exponential decay, yielding a Lorenzian line for the spectral density. Open circles: the correlation function is a KWW function with $\beta = 0.5$, resulting in a broadening of the spectral density and a shift of its maximum (eq 6). (c) Conversion of the widths parameter of a KWW function, β, to the width of a Gaussian distribution of exponential decays, δ.

FT of the correlation function yields the spectral density of motion, $I(\omega)$. In case of a single-exponential correlation function, the spectral density is a Lorentzian line, centered around $\nu_{MAX} = \omega_{MAX}/2\pi$ with a full width at half-maximum height (fwhmh) $\delta\nu$ of about 1.4 frequency decades. A value of $\beta < 1$ shifts the maximum according to[41]

$$\ln(2\pi\nu_{MAX}\tau_c) = 0.60607(\beta - 1) \quad (6)$$

and broadens the spectral density. Parts a and b of Figure 3 show schematic correlation functions and their corresponding spectral densities for $\beta = 1$ and 0.5, respectively. In discussions of NMR results, the distribution of correlation times is commonly assumed to be a logarithmic Gaussian distribution.[10] Since the widths of relaxation-time spectra (i.e., $L(\tau)$ or $H(\tau)$ in shear spectroscopy) can be used to quantify nonexponential

processes in relaxation spectroscopy, we correlate in Figure 3b the values of the time-domain parameter β with the widths of a log-Gaussian distribution. The plot was obtained by calculating exchange decays of the form

$$\frac{S}{S_0}(t_m, \tau_0, \delta) = \int_{-\infty}^{\infty} \frac{1}{\sqrt{2\pi}\delta} \exp\left[-\frac{\left(\ln\frac{\tau_c}{\tau_0}\right)^2}{2\delta^2}\right] \exp\left(-\frac{t_m}{\tau_c}\right) d(\ln \tau_c) \quad (7)$$

and extract the relation between the parameters β and δ by fitting data from eq 7 to eq 5. In the activation diagrams below (Figures 7, 11, and 13), we will quantify the dynamic processes obtained from NMR by ν_{MAX} and the widths of the distribution δ, indicated by vertical bars.

The CODEX experiments permit the estimation of both the time constant as well as the geometry of the dynamic process. The former is done by recording t_m dependent experiments for a sufficient large CSA recoupling (a sufficiently large number of π pulses) while the latter is accomplished by acquiring experiments in dependence of the CSA recoupling efficiency at a fixed value of t_m which must fulfill the condition $t_m \gg \tau_c$. The recoupling efficiency depends on the product of MAS-rotation period T_R, number of recoupling cycles N and CSA (in frequency units) $\nu_0\Delta\sigma$, $\nu_0\Delta\sigma NT_R$. From the asymptotic level of

$$\frac{S}{S_0}(\nu_0\Delta\sigma NT_R)$$

for $\nu_0\Delta\sigma NT_R \rightarrow \infty$ one can obtain the number of sites that are involved in the process, provided that all spins participate, while from the approach of

$$\frac{S}{S_0}(\nu_0\Delta\sigma NT_R)$$

toward this value, information about the jump angles can be obtained.[28] In general, a small-angle motion results in a slow increase of

$$\frac{S}{S_0}(\nu_0\Delta\sigma NT_R)$$

while for large-angle motions, the value

$$\frac{S}{S_0}(\nu_0\Delta\sigma NT_R)$$

reaches its asymptotic value at relatively small values of $\nu_0\Delta\sigma NT_R$. In practice, one might need to run a number of test experiments at different values of $\nu_0\Delta\sigma NT_R$ as well as t_m to make sure that the ultimate experiment is performed under proper conditions. However, it might happen that the experimental conditions do not allow to set these proper condition, for example, if the dynamic process is not fast enough to meet the limit $t_m \gg \tau_c$ at a specific temperature. In such cases, care must be taken not to be mislead by the experimental results.

Another effect appears us worth being mentioned: in the case of a distribution of motional amplitudes, the NT_R dependence as explained above acts as a dynamic filter. An experiment performed at short values of NT_R efficiently suppresses the contributions of small-angle processes to the experimental exchange decay. If the different motional amplitudes come along with different correlation times, the shape of the exchange decay (in addition to the plateau value) might become NT_R dependent. On one hand, this provides a tool to study the relation between a distribution of motional amplitudes and a distribution of correlation times. However, on the other hand, it complicates the comparison of NMR data with other experimental results. For that reason and since the purpose of the paper is to trace the contributions of different subunits to the overall relaxation behavior, we disregarded this subtle effect and performed all dependencies at a fixed NT_R value. Work to explore this effect is in progress and will be published elsewhere.

Separation of Spin-Exchange

The NMR exchange experiment detects whether the orientation of the probe nucleus before and after the mixing time has changed. It is completely irrelevant whether the molecule to which the nucleus belongs has reoriented during t_m or if the magnetization has been transferred from one nucleus to another by dipolar interaction. The latter is commonly termed spin diffusion and cannot be separated in the experimental exchange spectra from the desired effect of molecular reorientation. In general, both processes will be present in the exchange data. In Figure 1, we show an idealized schematic exchange decay. The full symbols exhibits a decay due to a molecular process at short t_m, a decay due to spin diffusion at longer t_m and the T_1 relaxation. The latter can be determined by an independent quick T_1 experiment or is being canceled by a reference experiment, see above. The time constant of spin diffusion τ_{SD} is typically on the order of some seconds in organic solids at natural ^{13}C isotopic abundance. However, this means that a detectable decay due to spin diffusion appears already at t_m of less than 100 ms! Detectable are decays with an exchange intensity that is at least comparable to the signal-to-noise. For selectively enriched substances, the decay due to spin diffusion happens at even shorter t_m (triangles in Figure 1). Given that the shortest value of t_m is on the order of one T_R which in turn is on the order of some hundreds of μs, the overall dynamic range of MAS exchange experiments is limited to just 2−3 t_m decades. Considering the fact that the decay even for a single-exponential function stretches over about 2 t_m decades (and over a much wider range for stretched exponential functions that are typically observed in polymeric systems), it becomes clear that the presence of spin diffusion seriously restricts the applicability of the method. The spin-diffusion decay often superposes with the T_1 decay. However, it is clear that the restricting process on the dynamic range in most practically relevant cases is not the T_1 but the spin diffusion: in fact, there are substances with T_1 as long as some thousands of seconds but still exhibiting dynamic processes detectable by MAS−NMR exchange techniques[42] (circles in Figure 1). Without the disturbing effect of spin diffusion, the dynamic range could be as large as 6 t_m decades while in practice, it shrinks down to 2−3 frequency decades. Another aspect is worth to be mentioned: in cases when τ_c is similar to τ_{SD}, the decays due to molecular exchange and spin diffusion superpose each other such that they do not appear as separate decays. This can at least

falsify the extracted dynamic parameters. Thus, we found ourselves encouraged to study the mechanism of spin diffusion and to find measures to either decrease its influence or to correct the experimental data such that only the effect of molecular reorientations remains.

The easiest way to separate contributions of molecular reorientation from spin diffusion is to utilize their different temperature dependencies. Molecular processes are commonly thermally activated, and thus, their time constants exhibit a temperature dependence while the spin diffusion is temperature independent in good approximation in the regime of interest. For smaller molecules like molecular crystals, the temperature dependence of the molecular process is given often by the well-known Arrhenius law. In polymers this is only the case for secondary relaxations while dynamic glass transitions (α processes) follow a typical non-Arrhenius behavior. The way to separate spin dynamics from molecular processes is to acquire exchange data at different temperatures, determine the time constants and assign them to either process. However, this simple approach works only for $\tau_c \ll \tau_{SD}$. Because τ_{SD} is about 1 s and the shortest possible t_m is about 1 ms, the temperature range in which τ_c fits in this window is rather narrow and the separation procedure becomes ambiguous. Nevertheless, there are cases in which this approach was successfully applied.[2,25]

A more elaborate approach is to establish experimental conditions under which the effect of spin diffusion is highly reduced. For solid-state ^{13}C-MAS NMR experiments on samples at natural isotopic abundance, the situation for nonprotonated carbons (carboxyl carbons) can be described as "$N = 0$ rotational resonance".[24] Under this condition, τ_{SD} for this case should increase with increasing MAS rate[43] which was recently demonstrated experimentally[44] and seems to open a way out of the dilemma. However, it requires MAS rates beyond 20 kHz which can be obtained only with dedicated MAS probes and by using small-diameter MAS rotors which in turn accommodate as little as 10 mg of material. With such little material, a sufficient signal-to-noise can be obtained only with unacceptable large number of signal accumulations, even so the better rf performance of this NMR probes compensates in part the smaller number of spins in the sample. For protonated carbons (aliphatic, aromatic), however, the SD mechanism is "proton-driven ^{13}C spin diffusion",[45] and it was shown that even at a MAS rate of 28 kHz, no reduction of the spin-diffusion efficiency was obtained.[44] One might be tempted to control the efficiency of spin diffusion by disrupting the ^{1}H−^{13}C coupling by applying ^{1}H decoupling during t_m, however, this only leads to a counterproductive effect, namely to an undesired shortening of τ_{SD}.[8] To our knowledge, there is currently no feasible approach to reduce the effect of spin-diffusion for protonated carbons in natural abundance systems efficiently.

The only possible way that remains is to subtract the effect of spin diffusion from the experimental obtained exchange decays that contains the effect of both molecular reorientations and spin diffusion. To do so, we first have to calculate how the two processes show up in the exchange decay of the ssb of order N, $s^N(t_m)$. We have to recall that spin-diffusion is a multisite process in which each carbon in the sample is coupled to all other carbons in close proximity by dipolar interaction and that its strength depends on the mutual distance. Such models has been treated in the past,[16] however, they

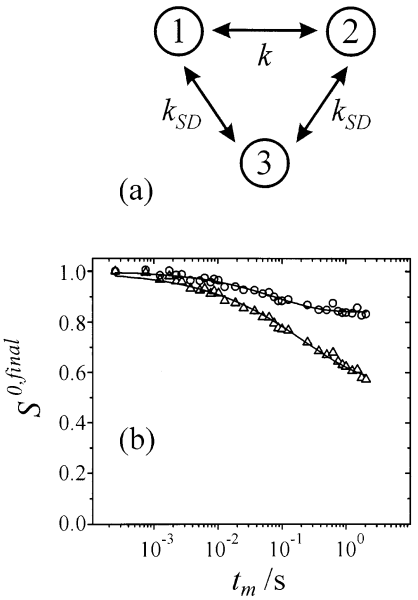

Figure 4. (a) Schematic exchange pathway for the spin-diffusion correction. Sites 1 and 2 are accessible by a molecular dynamic process with rate k while both sites are coupled to a site 3 by spin diffusion, rate k_{SD}. Site 3 stands for all other carbon spins that interact with the probe spin in site 1 or 2 via dipolar interaction. (b) Experimental exchange decays before and after SD correction: carboxyl resonance, trODESSA experiment, $\nu_R = 2.0$ kHz, and $t = -15$ °C.

are unfeasible for our case due to the large dimension of the resulting matrices and the lack of knowledge of the exact positions of interaction nuclei in the amorphous polymers. To have a practical recipe we assume as a schematic exchange pathway a three-site model: sites 1 and 2 are the sites that can be accessed by a molecular-exchange process; the jump rate between the two sites should be k. A third site, representing all other carbons, is coupled to both of the other sites by spin-diffusion with the rate k_{SD}. The corresponding exchange pathway is schematically shown in Figure 4a. Thus, the exchange matrix $\vec{\vec{K}}$ acquires the form

$$\vec{\vec{K}} = \begin{pmatrix} -k - k_{SD} - (1/T_1) & k & k_{SD} \\ k & -k - k_{SD} - (1/T_1) & k_{SD} \\ k_{SD} & k_{SD} & -2k_{SD} - (1/T_1) \end{pmatrix} \quad (8)$$

Its solution is given by

$$s^N(t_m) = (A^N + B^N e^{-3k_{SD}t_m} + C^N e^{-(k_{SD}+2k)t_m}) e^{-t_m/T_1} \quad (9)$$

where the parameters A^N, B^N, and C^N depend on the mutual orientations of the CSA tensors of the carbons at the different sites. This information is normally not available in disordered systems like amorphous polymers. We will thus treat the preexponential parameters as fitting parameters only.

To cast eq 9 into a more suitable form, we have to remind ourselves that spin-diffusion is actually a multisite process for which the parameter A^N becomes very small and that the spin-diffusion decay cannot be described by a single-exponential function anymore. Instead, we will use the well-known KWW function.[39]

Together with the re-definition

$$\tau_c = \frac{1}{2k} \quad \text{and} \quad \tau_{SD} = \frac{1}{k_{SD}}$$

eq 9 becomes

$$s^N(t_m) = (B^N e^{-3(t_m/\tau_{SD})^\beta} + C^N e^{-(t_m/\tau_{SD})^\beta} e^{-(t_m/\tau_c)}) e^{-t_m/T_1} \quad (10)$$

where β ($0 < \beta \leq 1$) is a measure of the widths of the spin-diffusion time constants, caused by the distribution of distances between the spins. Normally, β is on the order of 0.6−0.7[8,42,46] which in turn means that we can replace in eq 10 $e^{-3(t_m/\tau_{SD})^\beta}$ by $e^{-(t_m/\tau_{SD})^\beta}$ as a rough approximation. In fact, the factor 3 in the first exponential of eq 10 depends on the choice of the schematic spin-diffusion model, i.e., it originates from the schematic three-site model that we have arbitrarily chosen above and has no real physical significance. If we now perform an exchange experiments at such low temperatures that there is no effect of molecular dynamics in the experimental decay, we are able to determine the term $e^{-(t_m/\tau_{SD})^\beta}$ experimentally. Dividing the experimental data taken at any temperature, which are affected by both spin diffusion and molecular exchange and can be described by eq 10, by the experimentally determined spin-diffusion decay $e^{-(t_m/\tau_{SD})^\beta}$ yields the SD-corrected exchange decay

$$s^{N,\text{corrected}}(t_m) = (B^N + C^N e^{-(t_m/\tau_c)}) e^{-(t_m/T_1)} \quad (11)$$

from which we can determine the relative amplitude of the exchange component $a^N = C^N/(C^N + B^N)$ and the correlation time of the molecular process, τ_c. The additional T_1 decay can either be eliminated by running a reference experiment or by dividing eq 11 by $e^{-(t_m/T_1)}$ obtained from a separate T_1 experiment (see above). The final expression is

$$S^{N,\text{final}}(t_m) = B^N + C^N e^{-(t_m/\tau_c)}. \quad (12)$$

Figure 4b compares data according to eqs 10 and 11, i.e., before and after the spin-diffusion correction. The exponential term $e^{-(t_m/\tau_c)}$ in eq 11 is actually replaced by a KWW term to account for the distribution of correlation times in amorphous systems; see below.

Results and Discussion

Figure 5 shows a CPMAS spectrum of PnHMA at $t =$ 25 °C, taken at a spinning rate of 3 kHz. The line assignment is given at the molecular structure of the monomeric unit in the insert. It can be seen that lines belonging to both the main chain (line no. 2) as well as to the side chain (line no. 3) can be separated; i.e., they can be used to gain detailed dynamic information about these substructures of the molecule by MAS NMR methods. In addition, the carboxyl carbon (COO), which links these substructures, can be exploited, too. Closer inspection reveals that the resonance line of the latter is well separated and has a CSA of about 155 ppm that is indicated by the strong ssb. Note that the $N = 1$ ssb is larger than the $N = 0$ one; i.e., the central line appearing at the resonance frequency equal to the isotropic chemical shift. In addition, the widths of the resonance line is about 800 Hz, which is most likely due to the amorphous structure of the material, i.e., it is due to a superposition of slightly different isotropic chemical shift of carbons in different environments of the amorphous structure of the polymer. These properties make the carboxyl carbon a perfect candidate for the application of the trODESSA technique. On the other hand, the aliphatic resonances no. 2 and no. 3 are relatively narrow (the line widths are about 150 and 400 Hz, respectively) but appear in a spectral range that is crowded with other resonance lines. In addition, their CSA is much narrower as compared to the carboxyl line. This becomes obvious from the very weak ssb in the aliphatic region of Figure 5. The latter two issues require a minimum MAS-spin rate of about 3.5 kHz to avoid overlap between the ssb belonging to different aliphatic lines. Thus, the dynamic behavior of these resonance lines requires the application of the CODEX technique. In fact, as we will see below, the signal-to-noise even after application of as many as five π-pulses evolution cycles is sufficiently good while the application of CODEX to the carboxyl line results in very noisy exchange decays from which a faithful extraction of dynamic parameters is impossible.

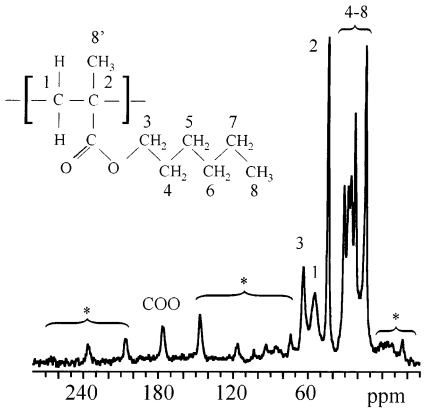

Figure 5. Monomer unit and MAS spectrum ($\nu_R = 3.0$ kHz, $t = 10$°C, 128 transients) of PHMA. The CSA values $\Delta\sigma$ were estimated as 45 ppm for carbon no. 3 (side chain), 28 ppm for carbon no. 2 (main chain) and 155 ppm for the carboxyl carbon. Spinning sidebands are marked with asterisks.

The upper limit of meaningful t_m values is either the value of the ^{13}C spin−lattice relaxation time T_1 or the onset of spin diffusion, whatever is shorter. The T_1 values for the different carbons at room temperature are 6.5, 3.1, and 0.31 s for the COO carbon, carbon no. 2 and carbon no. 3, respectively. These values vary by only about 20% in the temperature range of interest, emphasizing that there are no fast dynamic processes present. On the other hand, it is known that the characteristic spin-diffusion time τ_{SD} for ^{13}C nuclei in natural abundance is on the order of some seconds and the decay exhibit a wide distribution of τ_{SD}, due to the distribution of distances between the interacting spins.[8,16] It means that the spin-diffusion decay has already some effect on the exchange decay for t_m values as short as some hundreds of ms. Thus, a compensation for the effect of spin diffusion, as described above, is always necessary and was done for all the data presented here.

We would like to place a short comment here: it is the general impression of the authors that the effect of spin diffusion is often underestimated in MAS exchange experiments. We sometimes encountered the opinion that it is known from static experiments that spin diffusion does not show up until t_m values of some seconds. However, this argument neglects the fact that

Table 1. Correlation Times and Distribution Parameters, As Obtained from the Fitting of the Experimental Exchange Decay for the Three Carbons of Interest and for Different Temperatures[a]

	COO		C3 (side chain)		C2 (main chain)			
temp (K)	τ_c (ms)	β	τ_c (ms)	β	τ_c^1 (ms)	β^1	τ_c^2 (ms)	β^2
253			103 ± 52	0.67 ± 0.19	68 700	0.37 ± 0.12		
258	65 ± 13	0.43 ± 0.07						
263	118 ± 29	0.57 ± 0.12	31 ± 3	0.64 ± 0.05	6800 ± 135	0.73 ± 0.08	50 ± 5	0.67 ± 0.03
267	130 ± 17	0.41 ± 0.03						
273			20 ± 2	0.69 ± 0.07	1300 ± 50	0.59 ± 0.02	30 ± 2	0.78 ± 0.03
275	88 ± 8	0.41 ± 0.03						
279	52 ± 6	0.36 ± 0.03						
283	23 ± 2	0.36 ± 0.02	18 ± 1	0.62 ± 0.04	27 ± 5	0.64 ± 0.02	15 ± 1	0.87 ± 0.05
293	4 ± 1	0.52 ± 0.1	9 ± 1	0.82 ± 0.08	11 ± 3	0.68 ± 0.03	9 ± 1	0.96 ± 0.06

[a] The parameters for the COO carbon were obtained from trODESSA experiments, while data for C3 and C2 are from CODEX experiments.

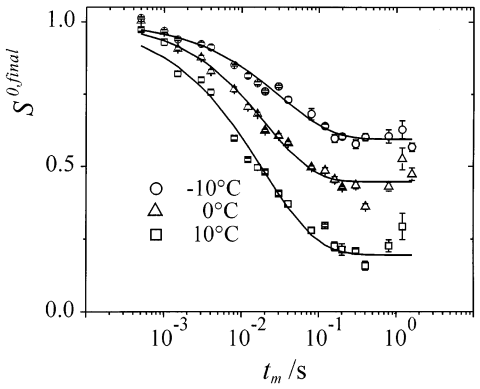

Figure 6. CODEX data (open squares) for side-chain carbon no. 3, depending on the length of the mixing period, t_m. ν_R = 2.0 kHz, and $\nu_0\Delta\sigma NT_R = 9.0$. The lines are best fits to eq 12; fit parameters are given in Table 1.

the sample rotation in MAS experiments at conventional frequencies provides a drastic enhancement of the efficiency of spin exchange.[8,45,47] The reason is that the rate of spin exchange depends strongly on the resonance frequency difference of the interaction spins: efficient spin exchange can only occur when the frequencies match each other. However, in an solidlike material and considering CSA, the resonance frequencies of two closely spaced carbon nuclei are in general different due to the different orientation of their CSA tensors. In MAS, on the other hand, these resonance frequencies become time-dependent and there are short periods during each MAS period when the two resonance frequencies of the interaction spins match each other ("level crossing"). During this period, even it is very short, a very efficient spin exchange occurs, shortening the spin-diffusion time τ_{SD} in MAS experiments considerably. Note that this effect can be exploited for structural investigations in cases where the spin-diffusion rate in static samples is very long and/or rather anisotropic.[48−51]

Figure 6 shows the CODEX exchange decays of the side-chain carbon no. 3 at selected temperatures, corrected for spin-diffusion and T_1. The different carbon atoms along the side chains probably exhibit different dynamic behavior and thus the amplitude and/or time scale might increase toward the end of the chains. However, since our aim is not the investigation of the motional heterogeneity along the side chains but rather to discriminate between the dynamics of different molecular segments, we choose the first carbon in the side chain (seen from the carboxyl group) as a representative. This choice was made based on considerations about spectral resolution and signal-to-noise ratio. The experiments were run with a value $\nu_0\Delta\sigma NT_R = 0.9$ and in normalized mode; i.e., the values of the intensities are normalized to vary between 0 and 1 by the experiment itself and are internally corrected for T_1. The error bars where calculated from the spectral signal-to-noise ratios of the exchange and normalization experiment. The increasing errors for t_m values larger than some hundreds of milliseconds are due to the signal decay by T_1 relaxation. A spin-diffusion correction was performed as described above. It can be seen that for all temperatures, the major share of the complete decay falls in the accessible t_m range, since the values $S^{N,final}(t_m)$ start at about 1 for short t_m and level off to a plateau for long t_m. Dynamic parameters obtained from the fitting of the data with eq 12 are listed in Table 1. It can be seen that the correlation time shortens with increasing temperature, as expected. Furthermore, the widths of the correlation time distribution, as indicated by the parameter β, is constant within the temperature range of the experiments. Calculated center frequencies and widths of the correlation time distributions are shown in the Arrhenius diagram of Figure 7. It may be seen that the NMR data match fairly those of the β process obtained from dielectric and shear experiments.[34] Therefore, we conclude that the side chain in PHMA contributes in the dynamic window of the NMR mainly to the β process. Since it is assumed to be a local process that does not involve larger segments of the molecule, this is not a very surprising result. Figure 6, however, also reveals that the plateau value $S^{0,final}(t_m \approx 1\ s) = 1 - a^0$ decreases with increasing temperature. This could be explained by (i) an increase in the number of sites involved in the process and/or an increase of the mobile fraction of spin, or by (ii) a change of the geometry such that the jump process involves larger angles with increasing temperature (remember that all experiments were performed at the same value of $\nu_0\Delta\sigma NT_R$). The question which explanation is the correct one can be answered by running exchange experiments as a function of number of recoupling cycles, $\nu_0\Delta\sigma NT_R$, at a fixed value of t_m (Figure 8a). It can be seen that for all temperatures, the asymptotic values of $S^{0,final}(\nu_0\Delta\sigma NT_R)$ is close to zero ($1 - a^0 \approx 0$), which means that the process involves a large number of sites, i.e., it has either a diffusive character (small-angle reorientations) or the topology is poorly defined (large-angle flips around varying jump angles, i.e., between a large number of possible sites). However, the approach toward this value happens for higher temperatures at shorter values of $\nu_0\Delta\sigma NT_R$, which means that the reorientation angles, i.e., the amplitude of motion, increase.[28,29] In principle, quantitative information about the values of

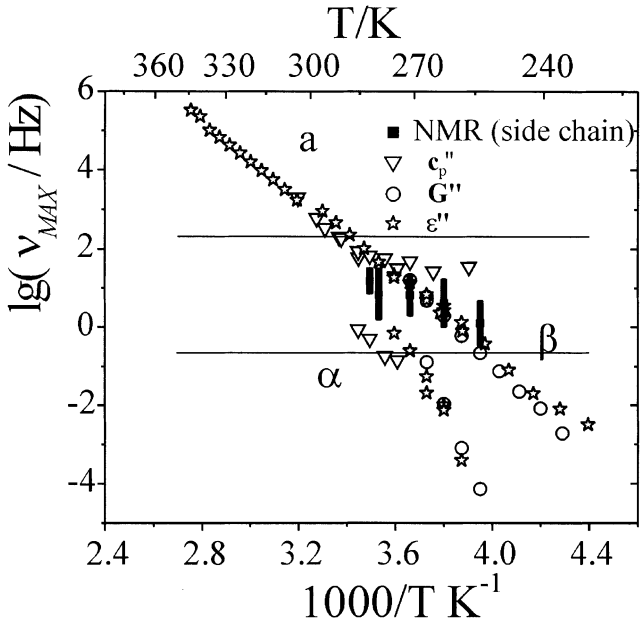

Figure 7. Arrhenius diagram for PHMA including the NMR results from the side-chain carbon (full squares). Open symbols are results from relaxation experiments[55] (triangle, heat-capacity spectroscopy; circles, mechanical relaxation; stars, dielectric relaxation). The widths of the correlation−time distribution, as obtained from the β parameter of the KWW fitting, are given as vertical bars.

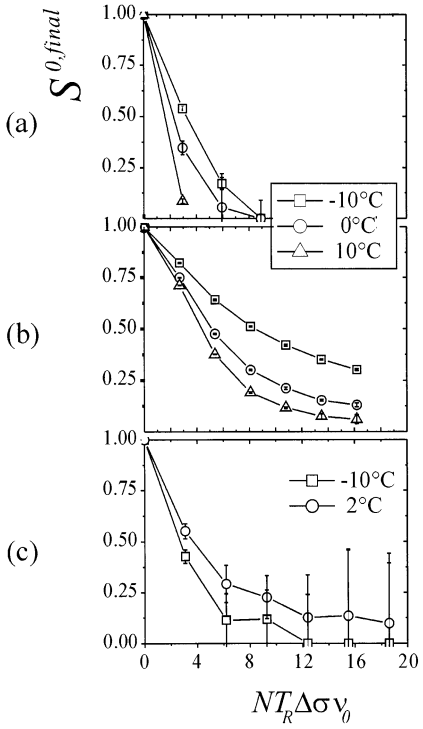

Figure 8. CODEX data (open squares) for all carbons, depending on the length of the evolution periods, $\nu_0\Delta\sigma NT_R$. The lines are guides for the eyes. Key: (a) side-chain carbon no. 3, $t_m = 0.5$ s, $\nu_R = 3.0$ kHz; (b) main-chain carbon no. 2, $t_m = 0.5$ s, $\nu_R = 2.0$ kHz; (c) carboxyl carbon, $t_m = 0.82$s, $\nu_R = 5.0$ kHz.

these angles could be obtained by comparison with calculated data. However, since we are lacking information about the exact tensor orientations as well as the type of the process, such considerations are close to speculations, and thus, we did not perform them and restrict ourselves to qualitative statements.

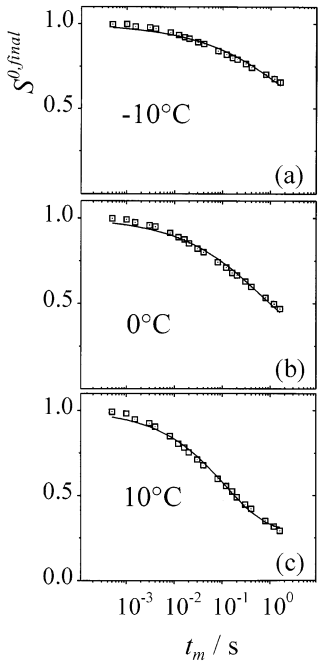

Figure 9. CODEX data (open squares) for main-chain carbon no. 2, depending on the length of the mixing period, t_m. $\nu_R = 2.0$ kHz, $\nu_0\Delta\sigma NT_R = 5.6$. The lines are best fits to eq 12, fit parameters are given in Table 1. Note the much better signal-to-noise ratio, as compared to Figure 6, and the deviation of the fitting from the experimental results. Experimental uncertainties are smaller than the size of the symbols.

Figure 9 show the exchange decays $S^{0,\text{final}}(t_m)$ for the main-chain carbon no. 2, extracted from the same NMR data sets as Figure 6. In contrast to the plots shown in Figure 6, the exchange decays at the lower temperatures could not be acquired down to the asymptotic value, due to the onset of spin-diffusion and T_1 relaxation at t_m values larger than about one second. However, the data taken at $t = 10$ °C indicate an exchange intensity of $a^0 \approx 0.75$. Taking this number as a fixed value for the fitting procedure and applying this number to the data taken at lower temperatures, too, one obtains curves as shown in Figure 9. A closer inspection reveals, however, that there is a substantial deviation of the experimental data from the fitted curves, in particular at t_m values around 10 ms. Considering the excellent signal-to-noise ratio, this deviation cannot be attributed to spectral noise but must be considered as a systematical deviation. Thus, we may suppose that the exchange decay of the main-chain carbon no. 2 is determined by more than one process. To verify this, we plotted in Figure 10 the difference of the experimental data and the fitted curve. The characteristic shape of this difference, together with the small scatter of the points, is a strong support for our assumption. Figure 10 (bottom right) shows the difference plot for a fitting function of type eq 12 but with two KWW functions. To reduce the number of free parameters and provide a more stable and reliable fit, we set the relative amplitude of the shorter component to 0.3, as suggested by the experimental data. The dynamic parameters are summarized in Table 1 and displayed in Figure 11. It may be seen that the parameters of the two spectral densities match those of the α and β processes which were obtained by relaxation methods. This indicates that the main-chain carbon no. 2 feels both contributions of localized motions (β) as well as more cooperative motions (α) that might involve a larger number of monomer units and that is indicated

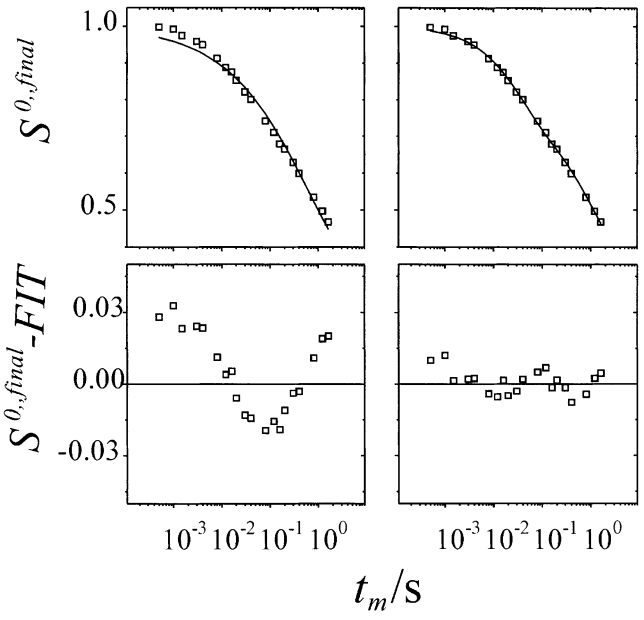

Figure 10. CODEX data (open squares) for main-chain carbon no. 2, depending on the length of the mixing period, t_m (top). They correspond to the center chart of Figure 8. The lines are best fits to either one (left) or two (right) KWW functions. The difference between experimental points and corresponding fits is shown below (difference plots). Note the characteristic shape of the difference plot for the case of a single and its relatively flat shape for the case of two KWW functions.

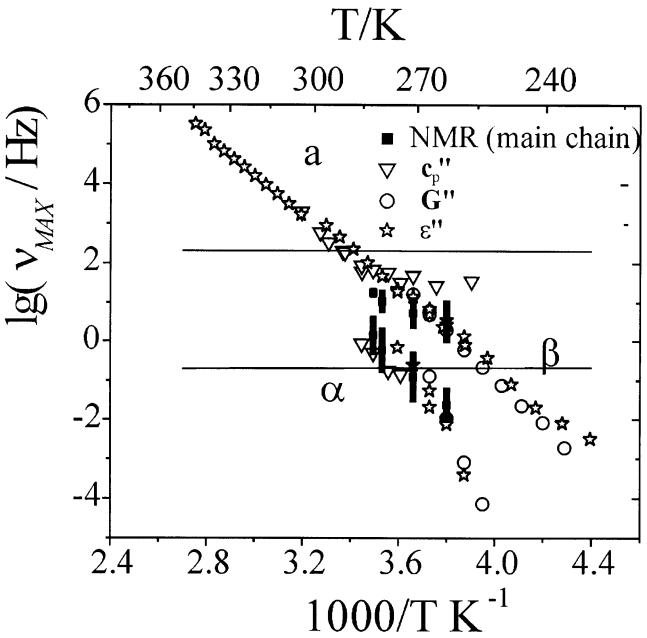

Figure 11. Arrhenius diagram for PHMA with the NMR results for the main-chain carbon (full squares) and results from relaxation experiments. The widths of the correlation-time distribution, as obtained from the β parameter of the KWW fitting, are given as vertical bars.

by its non-Arrhenius temperature dependence in relaxation spectroscopy data.

Similar to the side-chain carbon no. 3, we run again an exchange experiment in dependence on the CSA recoupling, $S^{0,\mathrm{final}}(\nu_0\Delta\sigma NT_R)$. We set $t_m = 0.5$ s which means that the condition $t_m \gg \tau_c$ is fulfilled for the faster dynamic process only. Thus, the following conclusions are valid for the contribution of the β process to the dynamics of the main-chain only. The result is shown in Figure 8b. It may be seen that although the asymptotic value $S^{0,\mathrm{final}}(\nu_0\Delta\sigma NT_R \rightarrow \infty)$ keeps increasing with increasing temperature, the approach of $S^{0,\mathrm{final}}(\nu_0\Delta\sigma NT_R)$ to this value happens over the same $\nu_0\Delta\sigma NT_R$ range. This can most conveniently be seen in comparison with Figure 6: while for the latter data, the asymptotic value is reached faster for increasing temperatures, i.e., at shorter values of $\nu_0\Delta\sigma NT_R$, the data shown in Figure 8b reach 50% of the (temperature dependent) asymptotic value at $\nu_0\Delta\sigma NT_R \approx 0.1$ for all temperatures. This means that the amplitude of motion, i.e., the jump angle of the dynamic process does not change with temperature, as in contrast to the β process in the side chain. The decrease of the asymptotic value might indicate an increasing number of mobile main-chain segments. However, there is certainly also a contribution due to the varying ratio τ_c/t_m at different temperatures (or, in other words, due to the unavoidable violation of the condition $t_m \gg \tau_c$ which varies with the temperature). With increasing temperature, the experimental exchange decay has decayed at $t_m = 0.5$ s to a smaller asymptotic value, due to the shorter τ_c of the fast process. This transforms into a apparent smaller value of $(1 - a^0)$ in Figure 8b. It is impossible to tell the two effects apart. Thus, we will restrict ourselves to the statement that the jump angles of that main-chain dynamic process that contributes to the β process do not vary significantly with increasing temperature for the experimental temperature range. No significant information about the geometry of the main-chain contribution to the α process can be extracted from these data; however, from the different temperature dependence of the motional amplitudes, it is reasonable to assume that the contributions of main and side chains to the β process are of different natures. It would be interesting to extend the experiments to a wider temperature range, however, the limits are set on one hand to the spin-diffusion that dominates the exchange decay at lower temperatures and on the other hand by the onset of dynamic line broadening[52,53] that tells that the dynamic processes are so fast that the resonance frequencies are not longer constant during the evolution periods. Thus, eq 5 is no longer strictly valid, and the information content of the NMR data becomes more complex.[54]

We now turn to the molecular dynamic of the carboxyl group that links the side to the main chain. One might expect that the dynamic fingerprints of both molecular segments can be found using the COO carbon, too, and that the experiments performed utilizing this molecular group are characteristic for the entire monomer unit. This is in particular important for dielectric relaxation experiments that probe the dynamics of the dipoles localized at the carboxyl group and NMR experiments that utilize selective ^{13}C labeling of the carboxyl group.[32,33] We performed experiments by the alternative 1D-MAS exchange method trODESSA. In contrast to the aliphatic carbons discussed before, the line widths of the carboxyl carbon is as large as about 4 ppm which might lead to a decrease in signal intensity due to T_2 relaxation and pulse imperfections during the CODEX evolution cycles. However, the CSA is large (155 ppm) which means that a ratio of $\Delta\sigma/\nu_R$ reasonable for trODESSA experiments can be obtained easily by convenient MAS spin rates of some kHz. It is also known[30−33] that the motion of the carboxyl group in similar polymers (PMMA, PEMA) involves large-angle reorientations of the CSA tensor which means it is

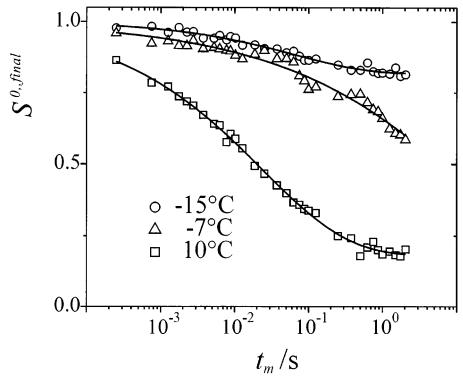

Figure 12. trODESSA data (open squares) for carboxyl carbon, depending on the length of the mixing period, t_m. ν_R = 2.0 kHz. The lines are best fits to eq 12, fit parameters are given in Table 1. Experimental uncertainties are smaller than the size of the symbols.

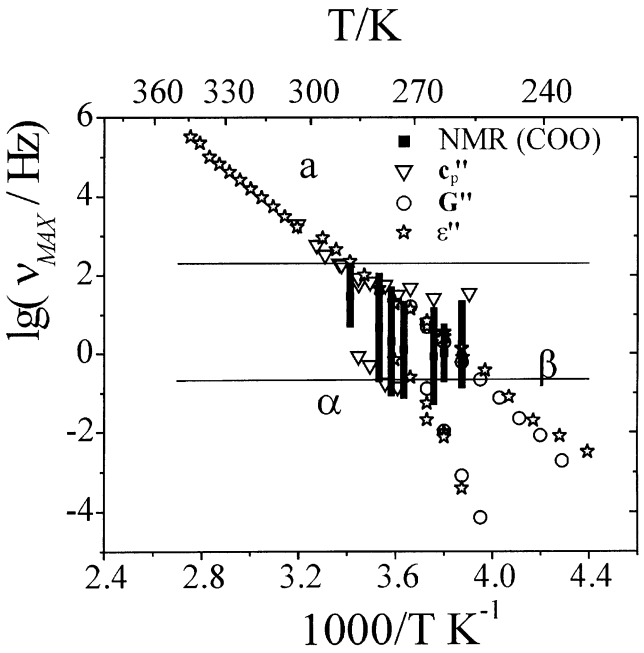

Figure 13. Arrhenius diagram for PHMA with the NMR results for the carboxyl carbon (full squares) and results from relaxation experiments. The widths of the correlation-time distribution, as obtained from the β parameter of the KWW fitting, is given as vertical bars.

desirable to switch to trODESSA experiments. Indeed, the CODEX-NT_R dependence shown in Figure 8c demonstrates that CODEX experiments at large values NT_R are less informative, since the signal intensity is much too low to provide a sufficient signal-to-noise. We thus turned to trODESSA experiments from which Figure 12 shows an exchange decay for different temperatures. We will first discuss the motional amplitude that exhibits itself in the plateau value $S^{0,\mathrm{final}}(t_m \approx 1\ \mathrm{s})$. It may be seen that there is only little exchange intensity a^0 of about 0.2 at $t = -15$ °C while for higher temperatures, a^0 is on the order of 0.8. Determination of the correlation times (see Table 1) and comparing them with relaxation data (Figure 13) reveals that the carboxyl dynamics at $t = -15$ °C is dominated by the β process while at higher temperatures, both α and β contribute significantly to the detected carboxyl dynamics. However, in contrast to the main-chain carbon no. 2 that also feels contributions from both α and β processes (Figure 11), and although the signal-to-noise ratios are comparable, we cannot tell the different processes apart in the carboxyl-exchange NMR data. This leads us to the conclusion that although the dynamic of the carboxyl carbon is influenced by α and β processes, its dynamic fingerprint is significantly different from both the main- and side-chain motions. It is not strictly justified to assign data obtained from the dynamics of this carbon to the dynamic of the entire monomeric unit.

It is interesting to compare the asymptotic level with corresponding calculations. It is known from experiments on PMMA and PEMA[30−33] that the carboxylic carbon performs a dynamics that can be characterized by the combination of a π-flip around the bond connecting the carboxyl carbon with the main-chain carbon no. 2 ("flip") and a rotation by an angle $\delta\gamma$ of the main-chain segment ("twist") around the C−C main-chain bond that adjusts for the violation of the local symmetry or by the latter only. Taking the tensor orientations and Euler angles from[33] and performing calculations as described in[27] yield an exchange intensity a^0 due to the "flip−twist combination" of about 0.44, much larger than the experimental value of 0.2 at low temperatures. In contrast, the result for the twist depends on the value of $\delta\gamma$ and yields 0.08 for $\delta\gamma = 10°$ and 0.20 for $\delta\gamma = 20°$. We conclude that the contribution of the carboxyl carbon to the β process, separated from the α process at lower temperatures, is more likely a small-angle twist of the main chain, rather than a "flip−twist combination" of the carboxyl group. At higher temperatures when the dynamics of the carboxyl carbon contributes to both the α as well as the β process, both motional models are likely to happen, as it was found for PMMA.[33] However, in contrast to PMMA where both the "flip" and the "twist" are assigned to the β process, we found that the "twist" only contributed to the β process. This might be attributed to the longer side chains of PHMA, as in contrast to the case of PMMA and PEMA: the shorter side chains, in combination with the detected "space-saving" motional model, permit a local process without substantial disturbance of the intermolecular environment. This might not be the case for PHMA. Thus, the "flip−twist combination" can only happen in the regime of the cooperative α process. This would mean in turn that the suggested model for PMMA/PEMA might not be applicable for PHMA. From our results, we can neither confirm nor reject this assumption finally. However, the only conclusion that can be drawn from both the value of the asymptotic trODESSA intensity as well as from the CODEX-NT_R dependence is that the "flip−twist combination" most likely involves a large-angle reorientation of the carboxyl carbon.

Summary

We performed a series of 1D-MAS exchange experiments on the amorphous polymer PHMA. The objective of this investigation was to assign the molecular dynamics of the different subunits of the monomer unit to the different relaxation processes that were detected by dielectrical and mechanical relaxation. The main chain was identified to contribute to both the α as well as to the β process while the side chain contributes in the dynamic window of NMR exchange experiments ($\tau_c \approx 1$ ms to 0.1 s) to the β process only. This can be interpreted such that the main chain performs a local as well as a cooperative dynamics while the side chain is not influenced significantly by the latter in the relevant time scales; i.e., the side chain preserves some dynamic independence from the main chain.[32] That

there is a coupling between the dynamics of both subunits anyhow, as found in similar polymers,[33] is emphasized by the fact that both contribute to the β process, as well as by the known dependence of the glass transition temperature on the length of the side chains.[34]

It has been shown that, for the extraction of quantitative results, it is crucial to correct the experimental data for the effect of spin exchange (SD). To our knowledge, there is no experimental tool yet to suppress its influence in real cases. We presented a procedure that compensates for its influence in good approximation and provides "SD-corrected" experimental data that contain the effect of molecular dynamic processes only.

This paper also demonstrates that for a comprehensive investigation of the molecular dynamics in polymeric systems, it is absolutely essential to combine the results obtained by different methods. The well-known relaxation methods feature a much wider dynamic range and a much better quality of the data (in terms of signal-to-noise); however, they are lacking molecular resolution as well as the opportunity to characterize the geometry of the dynamic processes. The latter can be provided by recent solid-state NMR methods, which, however, suffer from a limited frequency range and require a much bigger investment in hardware and experimental time.

Acknowledgment. We would like to thank Kay Saalwächter (Freiburg, Germany) and Horst Schneider, Günter Hempel, and Ernst Donth (Halle, Germany) for stimulating discussions. This work was supported by the Deutsche Forschungsgemeinschaft DFG in the framework of the Sonderforschungsbereich SFB 418.

Note Added after ASAP Posting

This article was released ASAP on 4/15/2003. In eqs 5 and 10 and in the paragraph following eq 10, the beta has been made superscript to the preceding term. The corrected version was posted 5/9/2003.

References and Notes

(1) Geil, B.; Isfort, O.; Boddenberg, B.; Favre, D. E.; Chmelka, B. F.; Fujara, F. *J. Chem. Phys.* **2002**, *116*, 2184−2193.
(2) Favre, D. E.; Schaefer, D. J.; Auerbach, S. M.; Chmelka, B. F. *Phys. Rev. Lett.* **1998**, *81*, 5852−5855.
(3) Dahmouche, K.; Atik, M.; Mello, N. C.; Bonagamba, T. J.; Panepucci, H.; Judeinstein, P.; Aegerter, M. A. *Sol. Energy Mater. Sol. Cells* **1998**, *54*, 1−8.
(4) Maxwell, A. S.; Ward, I. M.; Laupretre, F.; Monnerie, L. *Polymer* **1998**, *39*, 6835−6849.
(5) Palmer, A. G.; Williams, J.; McDermott, A. *J. Phys. Chem.* **1996**, *100*, 13293−13310.
(6) Krushelnitsky, A.; Reichert, D.; Hempel, G.; Fedotov, V.; Schneider, H.; Yagodina, L.; Schulga, A. *J. Magn. Reson.* **1999**, *138*, 244−255.
(7) Luz, Z.; Tekely, P.; Reichert, D. *Prog. NMR Spectosc.* **2002**, in press.
(8) Reichert, D.; Hempel, G.; Poupko, R.; Luz, Z.; Olejniczak, Z.; Tekely, P. *Solid State Nucl. Magn. Reson.* **1998**, *13*, 137−148.
(9) Jeener, J.; Meier, B. H.; Bachmann, P.; Ernst, R. R. *J. Chem. Phys.* **1979**, *71*(11), 4546−4553.
(10) Schmidt-Rohr, K.; Spiess H. W. *Multidimensional Solid-State NMR and Polymers*; Academic Press: San Diego, CA, 1994.
(11) Schmidt, C.; Blümich, B.; Wefing, S.; Kaufmann, S.; Spiess, H. W. *Ber. Bunsen-Ges. Phys. Chem.* **1987**, *91*, 1141−1145.
(12) Schmidt, C.; Blümich, B.; Spiess, H. W. *J. Magn. Reson.* **1988**, *79*, 269−290.
(13) Kentgens, A. P. M.; De Jong, A. F.; de Boer, E.; Veeman, W. S. *Macromolecules* **1985**, *18*, 1045−1048.
(14) Kentgens, A. P. M.; de Boer, E.; Veeman, W. S. *J. Chem. Phys.* **1987**, *87*, 6859−3832.
(15) Luz, Z.; Spiess, H. W.; Titman, J. J. *Isr. J. Chem.* **1992**, *32*, 145−160.
(16) Olender, Z.; Reichert, D.; Muller, A.; Zimmermann, H.; Poupko, R.; Luz, Z. *J. Magn. Reson. A* **1996**, *120*, 31−45.
(17) Weliky, D. P.; Tycko, R. *J. Am. Chem. Soc.* **1996**, *118*, 8487−8488.
(18) Jager, C.; Reichert, D.; Zimmermann, H.; Sen, T.; Poupko, R.; Luz, Z. *J. Magn. Reson.* **2001**, *153*, 227−237.
(19) Titman, J. J.; Luz, Z.; Spiess, H. W. *J. Am. Chem. Soc.* **1992**, *114*, 3756−3765.
(20) Domberger, W.; Reichert, D.; Garwe, F.; Schneider, H.; Donth, E. *J. Phys.: Condens. Matter* **1995**, *7*, 7419−7426.
(21) Yang, Y.; Schuster, M.; Blümich, B.; Spiess, H. W. *Chem. Phys. Lett.* **1987**, *139*, 239−243.
(22) Dixon, W. T. *J. Magn. Reson.* **1981**, *44*, 220−223.
(23) Dixon, W. T.; Schaefer, J.; Sefcik, M. D.; Stejskal, E. O.; McKay, R. A. *J. Magn. Reson.* **1982**, *49*, 341−345.
(24) Challoner, R.; Kümmerlen, J.; McDowell, C. *Mol. Phys.* **1994**, *83*, 687−700.
(25) Favre, D. E.; Schaefer, D. J.; Chmelka, B. F. *J. Magn. Reson.* **1998**, *134*, 261−279.
(26) Gerardy-Montouillout, V.; Malveau, C.; Tekely, P.; Olender, Z.; Luz, Z. *J. Magn. Reson.* **1996**, *A123*, 7−15.
(27) Reichert, D.; Zimmermann, H.; Tekely, P.; Poupko, R.; Luz, Z. *J. Magn. Reson.* **1997**, *125*, 245−258.
(28) DeAzevedo, E. R.; Hu, W. G.; Bonagamba, T. J.; Schmidt-Rohr, K. *J. Am. Chem. Soc.* **1999**, *121*, 8411−8412.
(29) DeAzevedo, E. R.; Hu, W. G.; Bonagamba, T. J.; Schmidt-Rohr, K. *J. Chem. Phys.* **2000**, *112*, 8988−9001.
(30) Kuebler, S. C.; Heuer, A.; Spiess, H. W. *Macromolecules* **1996**, *29*, 7089−7096.
(31) Kuebler, S. C.; Schaefer, D. J.; Boeffel, C.; Pawelzik, U.; Spiess, H. W. *Macromolecules* **1997**, *30*, 6597−6609.
(32) Kulik, A. S.; Beckham, H. W.; Schmidt-Rohr, K.; Radloff, D.; Pawelzik, U.; Boeffel, C.; Spiess, H. W. *Macromolecules* **1994**, *27*, 4746−4754.
(33) Schmidt-Rohr, K.; Kulik, A. S.; Beckham, H. W.; Ohlemacher, A.; Pawelzik, U.; Boeffel, C.; Spiess, H. W. *Macromolecules* **1994**, *27*, 4733−4745.
(34) Beiner, M. *Macromol. Rapid Commun.* **2001**, *22*, 869−895.
(35) Bielecki, A.; Burum, D. P. *J. Magn. Reson.* **1995**, *A116*, 215−220.
(36) Torchia, D. T. *J. Magn. Reson.* **1978**, *30*, 613−616.
(37) Bonagamba, T. J.; Becker-Guedes, F.; DeAzevedo, E. R.; Schmidt-Rohr, K. *J. Polym. Sci.: Polym. Phys. Ed.* **2001**, *39*, 2444−2453.
(38) Favre, D. E.; Schaefer, D. J.; Chmelka, B. F. *J. Magn. Reson.* **1998**, *134*, 261−279.
(39) Williams, E. D.; Watts, D. C. *Trans. Faraday Soc.* **1970**, *66*, 80−85.
(40) Laherrere, J.; Sornette, D. *Eur. Phys. J. B* **1998**, *2*, 525−539.
(41) Schröter, K.; Unger, R.; Reissig, S.; Garwe, F.; Kahle, S.; Beiner, M.; Donth, E. *Macromolecules* **1998**, *31*, 8966−8972.
(42) Reichert, D.; Hempel, G.; Zimmermann, H.; Tekely, P.; Poupko, R.; Luz, Z.; Favre, D. E.; Chmelka, B. F. *Appl. Magn. Reson.* **1999**, *17*, 315−327.
(43) Maricq, M. M.; Waugh, J. S. *J. Chem. Phys.* **1979**, *70*, 3300−3316.
(44) Reichert, D.; Bonagamba, T. J.; Schmidt-Rohr, K. *J. Magn. Reson.* **2001**, *151*, 129−135.
(45) Meier, B. H. *Adv. Magn. Opt. Reson.* **1994**, *18*, 1−116.
(46) Tekely, P.; Reichert, D.; Zimmermann, H.; Luz, Z. *J. Magn. Reson.* **2000**, *145*, 173−183.
(47) Ernst, M.; Meier, B. H. In *Solid State NMR of Polymers*; Ando, I., Asakura, T., Eds.; Elsevier: Amsterdam, 1998; p 83.
(48) Gan, Z. H.; Ernst, R. R. *Chem. Phys. Lett.* **1996**, *253*, 13−19.
(49) Gan, Z. H.; Robyr, P.; Ernst, R. R. *Chem. Phys. Lett.* **1998**, *283*, 262−268.
(50) Takegoshi, K.; Ito, M.; Terao, T. *Chem. Phys. Lett.* **1996**, *260*, 159−165.
(51) Reichert, D.; Mizumo, T.; Takegoshi, K.; Terao, T. *J. Magn. Reson.* **1999**, *139*, 308−313.
(52) Schmidt, A.; Smith, S.; Raleigh, D. P.; Roberts, J. E.; Griffin, R. G.; Vega, S. *J. Chem. Phys.* **1986**, *85*, 4248−4253.
(53) Reichert, D.; Hempel, G.; Zimmermann, H.; Schneider, H.; Luz, Z. *Solid-State NMR* **2000**, *18*, 17−36.
(54) Saalwächter, K.; Fischbach, I. *J. Magn. Reson.* **2002**, *157*, 17−30.
(55) Beiner, M.; Kahle, S.; Hempel, E.; Schröter, K.; Donth, E. *Macromolecules* **1998**, *31*, 8973−8980; *Europhys. Lett.* **1998**, *44*, 321−327.

MA0212442